Chemical Engineering Journal xxx (2016) xxx–xxx

Contents lists available at ScienceDirect

Chemical Engineering Journal

journal homepage: www.elsevier.com/locate/cej

Removal of VOCs by catalytic process. A study of MnZnO composites synthesized from waste alkaline and Zn/C batteries

María V. Gallegos [a], Miguel A. Peluso [a], Elisabetta Finocchio [b], Horacio J. Thomas [a,c], Guido Busca [b], Jorge E. Sambeth [a,*]

[a] Centro de Investigación y Desarrollo en Ciencias Aplicadas, "Dr. Jorge J. Ronco" CINDECA (UNLP – CCT CONICET La Plata), 47 N257 La Plata, Buenos Aires, Argentina
[b] Dipartimento di Ingegneria Civile, Chimica e Ambientale, Università di Genova, Genova, Italy
[c] PlaPiMu – Planta Piloto Multipropósito, (CICPBA-UNLP) Cno. Centenario y 505, M.B. Gonnet, Buenos Aires, Argentina

HIGHLIGHTS

- Synthesis of MnZnO composites as catalysts for ethanol and toluene oxidation.
- Recovery of zinc and manganese from alkaline and zinc-carbon spent batteries.
- The better performance of MnOx is due to the higher Mn/Zn ratio and the absence of ZnO.
- FTIR show that ethanol is adsorbed to form ethoxy and acetate species.
- Benzene (g) → Benzyl (a), Benzoate (a) → CO_2.

GRAPHICAL ABSTRACT

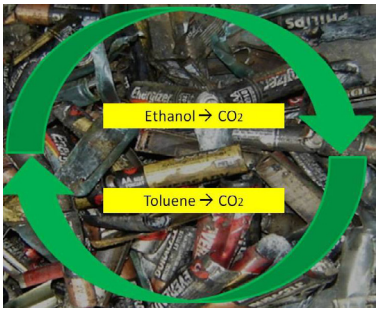

ARTICLE INFO

Article history:
Received 16 July 2016
Received in revised form 5 October 2016
Accepted 1 November 2016
Available online xxxx

Keywords:
MnZn recyclin
Waste batteries
Catalytic combustion
VOC abatement
FTIR spectroscopy

ABSTRACT

Spent alkaline and zinc-carbon batteries were subjected to a biohydrometallurgy process, in order to recover manganese and mixed manganese zinc oxides. Two solids were synthesized, one of them prepared by reaction of $MnSO_4$ and $KMnO_4$ (MnO_x) and the other obtained by chemical precipitation with NaOH (ZnMnO).

The characterization by XRD, TPR, FTIR and XPS revealed the presence of Mn^{3+} and Mn^{4+} cations in both samples, and the presence of ZnO and Mn-Zn spinels in ZnMnO. The samples were evaluated in the oxidation reaction of ethanol and toluene. The results in the flow reactor showed that ethanol conversion on both catalysts, MnO_x and ZnMnO, is rather similar, but toluene conversion is markedly higher on MnO_x, due to a greater Mn/Zn ratio and to the absence of a crystallized ZnO phase. The FTIR study demonstrated that ethanol is oxidized to acetaldehyde at low temperature, and to CO_2 and CO at 400 °C. Traces of CH_4 in the gas phase are also detected at high temperature. The formation of ethoxy and acetate groups is observed at the catalyst surface. With respect to toluene oxidation, CO_2 is detected at 300 °C and when the temperature is increased, CO is also observed in the gas phase. The results showed that: (i) the alkaline and Zn-carbon batteries can be recycled as catalysts and (ii) the solids can be used in the catalytic process for VOCs control.

© 2016 Elsevier B.V. All rights reserved.

1. Introduction

Volatile Organic Compounds (VOCs) are recognized as major contributors to pollution and the photochemical formation of smog

* Corresponding author.
E-mail address: sambeth@quimica.unlp.edu.ar (J.E. Sambeth).

http://dx.doi.org/10.1016/j.cej.2016.11.001
1385-8947/© 2016 Elsevier B.V. All rights reserved.

Please cite this article in press as: M.V. Gallegos et al., Removal of VOCs by catalytic process. A study of MnZnO composites synthesized from waste alkaline and Zn/C batteries, Chem. Eng. J. (2016), http://dx.doi.org/10.1016/j.cej.2016.11.001

[1]. Catalytic oxidation using transition metal oxide based catalysts is an environment friendly and promising control technology for VOC emission remediation [2–4]. Among transition metal oxides used for VOC oxidation, manganese oxide based materials exhibit great potential [5–7]. On the other hand, ZnO is used as photocatalyst [8,9] and in different catalytic reactions, such as steam reforming of alcohols [10,11], synthesis of methanol [12] and complete oxidation of CO [13] and trichloroethylene [14]. Also, ZnO doping with transition metals such as Mn and Cu could affect the electronic surface band structure of ZnO and improve its catalytic applications [13,15,16].

Spent batteries represent a dangerous waste, mainly due to the presence of poisonous and pollutant heavy metals [17–19]. In particular, alkaline batteries contain Zn and Mn. Zinc and manganese are essential elements for plants, animals, and humans, but at high levels it is toxic to all organisms [20–22]. In many countries of the world, spent batteries are usually disposed of in landfills with the domestic garbage [23,24]. The recovery and reutilization of both Zn and Mn from batteries would be very beneficial [25], and a number of procedures have been proposed for their recovery from waste batteries. The two common routes used in Mn and Zn recovery from spent alkaline and Zn/C batteries [26] are pyrometallurgical and hydrometallurgical processes. Hydrometallurgical process has environmental advantages such as lower gas emissions and lower energy consumption [27].

In addition, spent alkaline and Zn/C batteries are used as raw materials for the synthesis of ferrites, where manganese and zinc are recuperated together, but this process include the adding of stoichiometric amounts of analytical reagents (Mn, Zn and Fe salts) to assure the desire final composition [28,29].

In a previous paper [30] we obtained a manganese oxide with interesting catalytic properties from spent batteries by electrolysis and by precipitation with $KMnO_4$. In the present work, after leaching of spent alkaline and Zn/C batteries in an acid-reductive medium, we studied a mixed zinc-manganese oxide obtained by co-precipitation with NaOH, and compared to a manganese oxide obtained after precipitation Mn^{2+} with $KMnO_4$. The solids obtained in this work were analyzed as possible catalysts for ethanol and toluene total oxidation. In addition, the reaction mechanism by FTIR spectroscopy of VOC oxidation onto the recuperated solid was also studied.

2. Experimental

2.1. Recovery of Mn-based materials from alkaline and Zn-C cells

The biohydrometallurgical process for the treatment of spent alkaline and Zn/C batteries has been described in a previous work [31]. Briefly, batteries were first cut transversely and separate components, washed with distilled water, filtered and dried, leaving a powder containing 34 wt% Mn and 22 wt% Zn. Leaching tests were performed using bio-generated sulfuric acid of pH = 0.80 (produced in an air-lift bioreactor type, filled with sulfur where a strain of Acidithiobacillus thiooxidans was inoculated [31]). Once completed the leaching step, the solution containing zinc and manganese were used for the synthesis of catalysts:

MnO_x: Over 100 mL of leached solution, 100 mL of $KMnO_4$ were added in order to react with $MnSO_4$. The solution was stirred for 30 min. The solid synthesized was filtered, washed with distilled water, dried at 120 °C and calcined in air at 500 °C for 2 h.

ZnMnO: 100 mL of NaOH was added dropwise to 100 mL of the leachate liquor until pH 8, and the suspension was stirred at 30 °C for 1 h. The product was filtered, washed with distilled water and dried at 120 °C for 24 h. Finally, the solid was calcined in air at 500 °C for 2 h.

2.2. Characterization and spectroscopic techniques

The samples were characterized by X-ray diffraction (XRD) using a Philips PW1390 Diffractometer. The X-ray beam used for diffraction analysis was CuKα radiation. The Scanning Electron Microscopy (SEM) studies were carried out using in a Phillips SEM 505 microscope. The quantitative and qualitative study was analyzed with an Energy Dispersive X-ray Spectroscopy (EDS), which is coupled to SEM equipment. X-ray photoelectron spectra (XPS) were recorded using a multitechnique system with Al Kα (1486.6 eV) emission as X-ray source. The textural properties were carried using a Micromeritics Accussorb 2100 D sorptometer. Specific surface area was obtained by BET method. Mn and Zn content were determined by atomic absorption spectrophotometry (AAS) using a Varian AA 240 spectrophotometer. FTIR spectroscopy studies were performed on a Bruker IFS66 infrared spectrometer at spectral resolution of 4 cm^{-1} accumulating 200 scans. The sample reducibility was analyzed by temperature programmed reduction (TPR) tests using a 5% H_2/N_2 reducing mixture carrier gas flowing at 22 cm^3 min^{-1}. The experiments were performed at a heating rate of 10 °C min^{-1} from room temperature to 900 °C using 50 mg of sample. Calibration was carried out with NiO.

2.3. Catalytic activity

The catalytic activity of the samples was evaluated by means of the ignition curves of ethanol and toluene in air. The experiments were carried out in a flow U-shape glass reactor at atmospheric pressure. 100 mg of catalyst was placed into the glass reactor and a reactive flow (2 vol% of VOC in air) was passed through it at total flow rate of 100 cm^3 min^{-1}, which gives a gas hourly space velocity of 36,000 h^{-1}. The reactants and products were measuring by GC-FID (Thermofinnigan Trace CG) together with CO_2 monitoring by an on-line detector (Telaire CO_2 sensor). The conversion of VOC (X) and the conversion into CO_2 (X_{CO2}) were respectively calculated as $X = 1 - F_{VOC}/F_{VOC,in}$ and $X_{CO2} = F_{CO2}/\nu F_{VOC,in}$, where F_{VOC} is the outlet molar flow rate of VOC at steady state, $F_{VOC,in}$ is the inlet molar flow rate of VOC, F_{CO2} is the outlet molar flow rate of CO_2 at steady state and ν is the number of carbon atoms in the VOC molecule (for ethanol and toluene, ν = 2 and 7, respectively). In the case of ethanol, the conversion into acetaldehyde (X_{acetal}) was calculated as $F_{acetal}/F_{VOC,in}$, where F_{acetal} is the outlet molar flow rate of acetaldehyde at steady state.

The ethanol ignition curve over the catalysts was also studied using N_2 in absence of air, in the same apparatus described above.

2.4. FTIR in situ

The surface chemistry study was performed by using Nicolet 380 FT-IR (Fourier transform infrared spectroscopy) spectrometers, with the pure powders pressed into self-supporting wafers (~30 mg).

The catalysts were activated in the IR cell connected with conventional gas-manipulation apparatus at 500 °C in air and under vacuum (10^{-4} torr). The activated samples were then contacted with ethanol or toluene vapor at room temperature (r.t) and at increasing temperatures up to 500 °C. In another set of experiments, air was admitted in the IR cell together with the organic compound. The IR analysis of surface species arising from organics oxidation as well as the analysis of gas phase species was carried out at each temperature.

Please cite this article in press as: M.V. Gallegos et al., Removal of VOCs by catalytic process. A study of MnZnO composites synthesized from waste alkaline and Zn/C batteries, Chem. Eng. J. (2016), http://dx.doi.org/10.1016/j.cej.2016.11.001

3. Results and discussion

3.1. Characterization of materials

By EDS analyses the sulfur content in the samples was less than 3 wt% for the MnO_x solids, and about 10 wt% for the ZnMnO solid.

The samples obtained from the leachate liquor after leaching of spent batteries contained both metals, Mn and Zn. The manganese/zinc ratio along with the specific area of the samples used is listed in Table 1. MnO_x presents a higher specific area than ZnMnO, possibly due to the formation of an α-MnO_2 oxide (see next paragraph). As can be seen, the surface area is of a similar order and the preparation techniques showed that the amount of Zn in ZnMnO catalyst is higher than that of MnO_x solid.

The X-ray diffraction patterns of the synthesized oxides are depicted in Fig. 1. The X-ray diffraction pattern of MnO_x presents diffraction lines corresponding to α-MnO_2 phase (JCPDS 44-1386) and additionally, some diffraction lines corresponding to Mn_2O_3 (Bixbyite JCPDS 89-4836) were detected. No peaks corresponding to ZnO or Mn-Zn mixed compound are found. On the other hand, in the ZnMnO sample, the diffraction lines corresponding to hexagonal ZnO wurtzite (JCPDF 36-1451) are observed. Additionally, small peaks corresponding to $ZnMnO_3$, Mn_2O_3 and λMnO_2 were detected.

SEM images of the synthesized oxides (Fig. not shown) indicated that the morphology of the solids obtained is in general rather similar.

The FT-IR spectrum of the oxides is shown in Fig.2. Two bands are detected at 506, 613 cm^{-1} assigned to stretching of Mn-O [32] and Mn-O-Zn [33], respectively. In addition, a broad band at around 1200 cm^{-1} is detected, characteristic of a S=O sulfate bonds [34].

In order to know about the chemical bonding structure of the oxides, the XPS spectra for the valence bonds of Mn $2p_{3/2}$, Zn $2p_{3/2}$ and O 1s states were recorded and are shown in Fig. 3. The corresponding binding energies of the above states are also listed in Table 2. The spectra of Zn $2p_{3/2}$ of the samples exhibit a symmetric single peak that could be nicely fitted to a single peak, ruling out the possibility of the existence of multiple components of Zn in these samples. The peak corresponding to Zn2p ions in MnO_x, shifted to lower binding energies compared to ZnMnO sample. Taking into account than the manganese percentage of MnO_x is higher than ZnMnO, this shift in binding energy is due to the ZnMn bonding structure [35], and to the different bonding states of the elements on the surface [36]. Zn atoms bonded to manganese (which are less electronegative than oxygen) will contribute to the shift of the Zn $2p_{3/2}$ peak [37].

For all the samples, the O1s peak is in general composed of three components centered at about 529, 530 and 532 eV. The lower binding energy (OI) is ascribed to lattice O, the medium binding energy peak (OII) is assigned to surface adsorbed O, OH^- groups and O vacancies [38] and the higher binding energy peak correspond to adsorbed molecular water. OII species have greater mobility than lattice oxygen (OI) and may give rise to beneficial spillover phenomena at the solid surface [6]. The OII/OI ratio is higher for MnO_x (0.67) than ZnMnO (0.42). Taking into account that OI species are nucleophilic reagents, they are usually considered responsible for selective oxidation reactions, although their participation to the first steps of catalytic combustion cannot be ruled out. On the other hand, OII oxygens are electrophilic species and are reported to be highly reactive for total oxidations reactions [39].

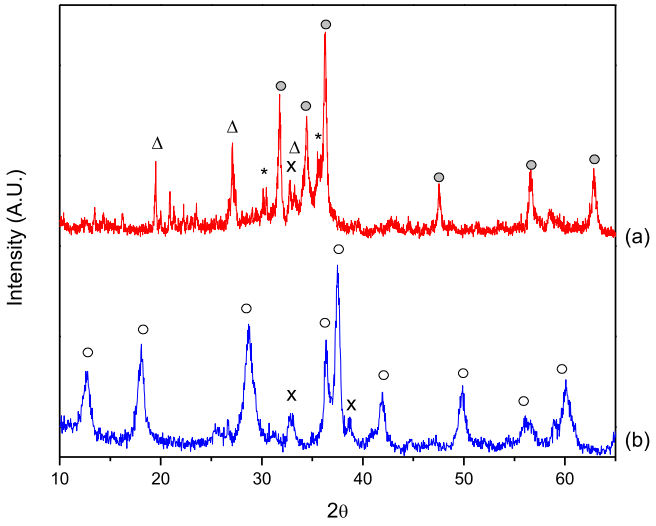

Fig. 1. X-ray diffraction patters of samples: (a) ZnMnO and (b) MnO_x. (x Mn_2O_3, o MnO_2, ◍ ZnO, ∗ $ZnMnO_3$, △ MnO_x).

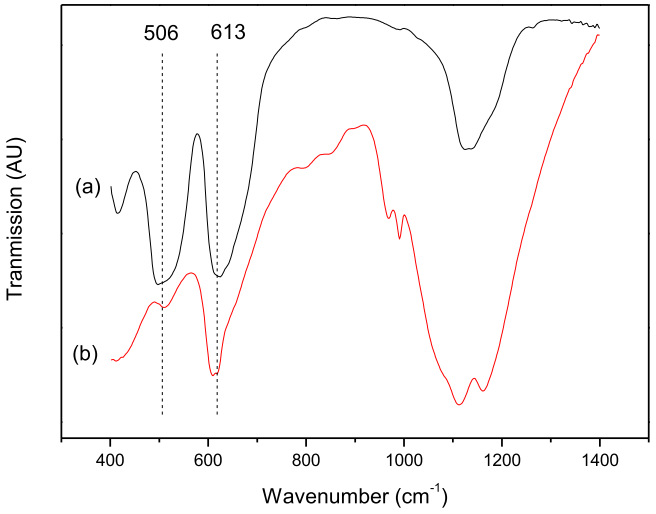

Fig. 2. FTIR skeletal spectra of samples: (a) ZnMnO and (b) MnO_x.

For the evaluation of the Mn valence state, the Mn$2p_{3/2}$ spectra were studied. Although the Mn 3 s level is usually used for the determination of the Mn oxidation state, this energy region was overshadowed by the presence of a very strong Zn 3p peak, and thus Mn 2p lines were analyzed instead. In both samples, MnO_x and ZnMnO, the Mn$2p_{3/2}$ peak level is centered near 642 eV, and could be deconvoluted into two Mn$2p_{3/2}$ components, which could be associated with Mn^{3+} and Mn^{4+} species [40].

The reduction behavior of the catalysts was followed by H_2-TPR, as shown in Fig. 4. It is assumed that MnO is the reduced state of

Table 1
Textural properties and composition of the samples.

Sample	SBET ($m^2\ g^{-1}$)	Vp ($cm^3\ g^{-1}$)	Mn/Zn EDS	Mn/Zn AA	TPR Area (a.u.)
ZnMnO	33	0.15	0.6	0.4	6.4
MnO_x	37	0.16	6.7	2.5	12.0

Please cite this article in press as: M.V. Gallegos et al., Removal of VOCs by catalytic process. A study of MnZnO composites synthesized from waste alkaline and Zn/C batteries, Chem. Eng. J. (2016), http://dx.doi.org/10.1016/j.cej.2016.11.001

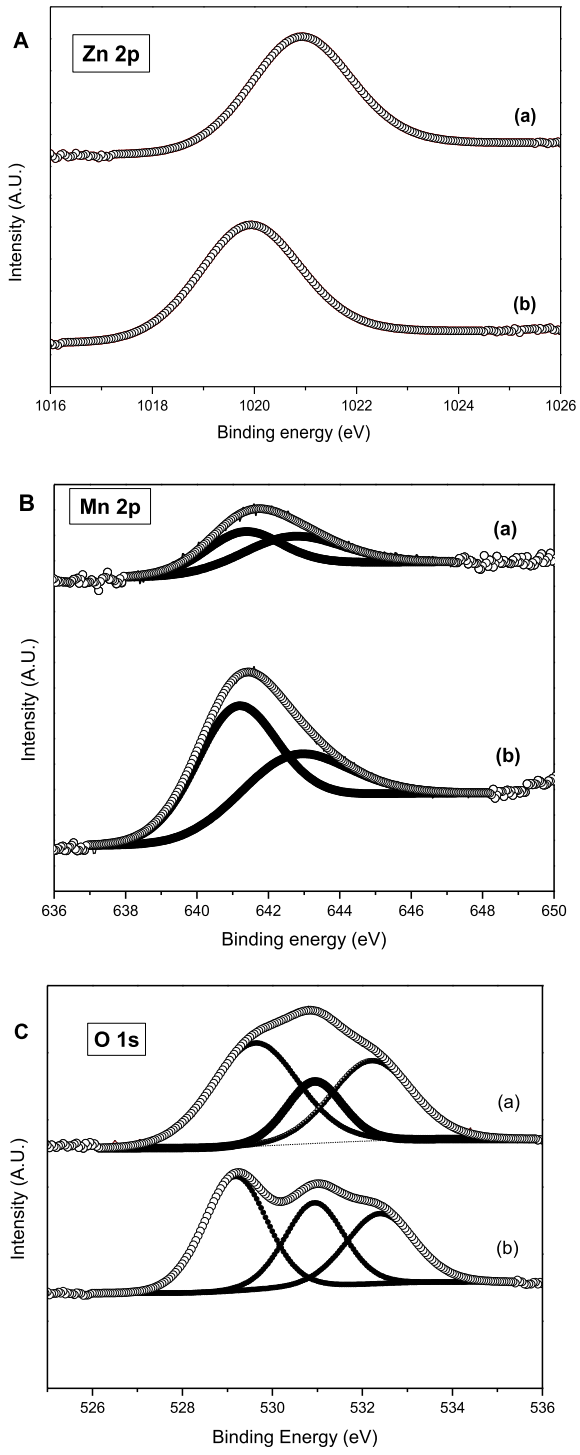

Fig. 3. XPS spectra of the (a) ZnMnO and (b) MnO_x samples in the Zn 2p (Section A), Mn 2p (Section B) and O 1s core level regions (Section C).

the MnO_x species above 800 °C [41]. As is illustrated in Fig. 4, in the TPR curve of the samples, there is one broad peak spanned within the temperature range of 200–600 °C. On both samples, the reduction starts at about 250 °C, and presents a maximum at 405 and 430 °C for MnO_x and ZnMnO, respectively. Taking into account that the reduction of ZnO starts at above 600 °C [42,43] the reduction peaks may consist of the following successive reduction steps: MnO_2 – Mn_2O_3 – Mn_3O_4 – MnO [44] or the reduction series Mn_5O_8 – Mn_2O_3 – Mn_3O_4 – MnO [45]. Additionally to the reduction steps described above, in ZnMnO sample, the reduction peaks may also include the reduction of the $ZnMnO_3$ phase, which reduction could be easier than that of MnO_x, due to the ZnO properties, as it was reported by Liang et al. [42].

Taking into account H_2 consumption in the samples, a manganese average oxidation state (AOS) of 3.8 and 3.7 was calculated for ZnMnO and MnO_x, respectively, which indicates the presence of manganese cations in different oxidation states.

3.2. Catalytic combustion data

The results of catalysts activity for ethanol oxidation in the presence of air are shown in Fig. 5 and Fig. 6. The T_{50} (temperature for 50% conversion) is 156 and 170 °C for ZnMnO and MnO_x respectively. These values of T_{50} are on the same order as the results obtained by different authors [46,47]. On the other hand, the T_{90} (temperature for 90% conversion) on ZnMnO is higher than the values reported in bibliography and is also higher than the MnO_x prepared in this work (Table 3).

In all cases, the main product is CO_2, but the formation of partial oxidation product of ethanol, namely acetaldehyde, has been detected. Figs. 6 and 7 show some formation of acetaldehyde on both catalysts, MnO_x and ZnMnO. The ethanol adsorption – oxidation could be divided in two parts; one of them between 0 and 50% and the other between 50 and 100% of conversion. In the first range ethanol conversion on ZnMnO catalyst is higher than in MnO_x (see Table 3). At high temperature the acetaldehyde production in both catalysts is detected. In MnO_x, acetaldehyde selectivity was 6% at 300 °C (more than 90% conversion), whereas in ZnMnO solid, acetaldehyde selectivity was 18% at 250 °C, were the ethanol conversion was 80%.

The ethanol ignition results in absence of air (N_2 Air Liquid 99.9%) can be seen in Figs. 5 and 6. The results showed that the conversion reached 20 and 10% at 300 °C on MnO_x and ZnMnO, respectively.

In Fig. 7 the light-off curves relative to toluene combustion in air on the two catalysts are compared. MnO_x is the most active one, showing high toluene conversion (≈70%) already at 350 °C, while at this temperature the ZnMnO catalyst the conversion is 40% only. In all cases the only product is CO_2, showing no by-product formation for this reaction.

When toluene is adsorbed on MnO_x, the aromatic ring became unstable and conducts to total oxidation to CO_2. Over manganese oxides with cryptomelane structure, Santos et al. [46] shown that adsorbed toluene affects the mobility of the oxygen species, making them less reactive and the oxide is able to retain toluene at high temperatures.

As remarked by Lüth et al. [48], oxygenated VOCs can be adsorbed strongly on oxide surfaces through coordination of their nonbonding oxygen electron pairs, thus they are more strongly chemisorbed than aromatic hydrocarbons that adsorb through their π-type C=C orbitals. For this reason, the activation energy of O-VOC combustion is lower than that of aromatic compounds. These results and our results allow us to say that the limited interaction VOCs–ZnO is mainly responsible for the different catalytic activity over each catalyst, for instance, the lower toluene conversion on the ZnMnO catalyst.

It has been reported that the activity of manganese oxides in the oxidation of VOCs is due to the presence of the Mn^{3+}–Mn^{4+} couple and the tunnel structure of the oxide [49,50]. On the other hand, some authors have also reported a correlation between the presence of the OII species and the catalytic activity, due to the higher mobility of the OII species compared to that of the OI species [51].

In our two catalysts, XPS results confirm the presence of the Mn^{3+}–Mn^{4+} couple and show that the concentration of OII species

Please cite this article in press as: M.V. Gallegos et al., Removal of VOCs by catalytic process. A study of MnZnO composites synthesized from waste alkaline and Zn/C batteries, Chem. Eng. J. (2016), http://dx.doi.org/10.1016/j.cej.2016.11.001

Table 2
XPS results of the oxides.

Catalysts	O 1 s			Mn $2p_{3/2}$			Zn 2p		
	BE(eV)	specie	%	BE(eV)	specie	%	BE(eV)	specie	%
ZnMnO	529.8	O^{2-}	48	642.8	Mn^{4+}	49	1021.0	Zn^{2+}	100
	531.7	OH^-	20	641.9	Mn^{3+}	51			
	532.6	H_2O	32						
MnO_x	529.4	O^{2-}	43	642.9	Mn^{4+}	35	1020.7	Zn^{2+}	100
	531.1	OH^-	29	641.3	Mn^{3+}	65			
	532.5	H_2O	28						

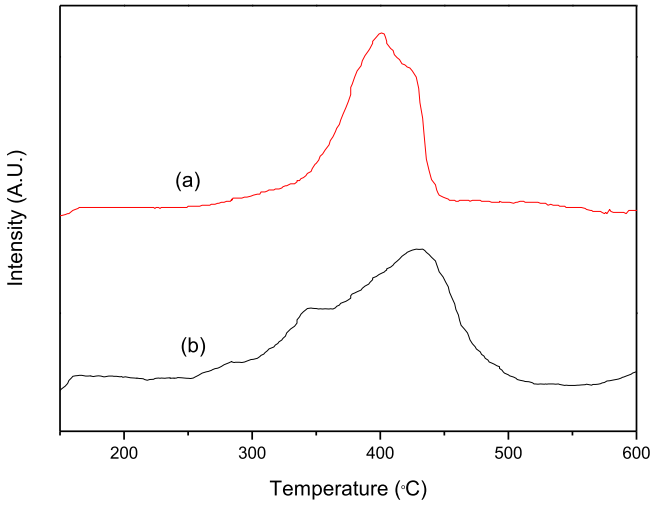

Fig. 4. TPR patterns of the oxides: (a) MnO_x and (b) ZnMnO.

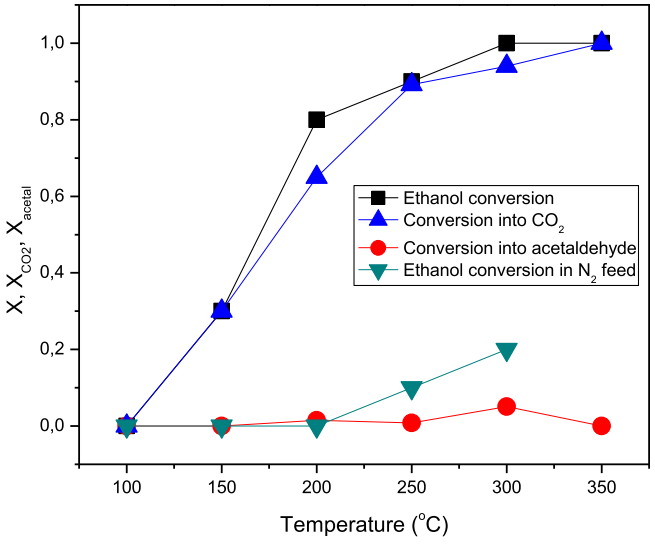

Fig. 5. Ethanol conversion, CO_2 yield, and acetaldehyde selectivity on MnO_x catalyst. ($X = 1 - F_{ethanol}/F_{ethanol,in}$, $X_{CO2} = F_{CO2}/2F_{ethanol,in}$, $X_{acetal} = F_{acetal}/F_{ethanol,in}$).

is slightly higher on MnO_x, possibly explaining the best ethanol and toluene conversions obtained on this catalyst.

In sum, taking into account that both catalysts present similar specific area, and contain Mn^{3+} and Mn^{4+}, the better performance of the MnO_x catalyst could be due to the higher Mn/Zn ratio and to the absence of a crystallized ZnO phase [13].

To have some more information, we compared the catalytic activity of these materials to those of an active manganese oxide

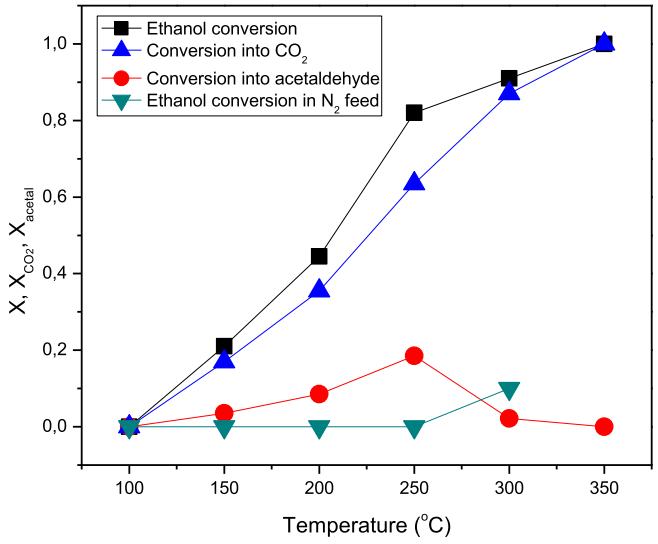

Fig. 6. Ethanol conversion, CO_2 yield, and acetaldehyde selectivity on ZnMnO catalyst. ($X = 1 - F_{ethanol}/F_{ethanol,in}$, $X_{CO2} = F_{CO2}/2F_{ethanol,in}$, $X_{acetal} = F_{acetal}/F_{ethanol,in}$).

Table 3
Ethanol and toluene conversion on ZnMnO and MnO_x catalysts.

Catalysts	Ethanol		Toluene
	T_{50} (°C)	T_{90} (°C)	T_{50} (°C)
ZnMnO	156	302	
MnO_x	170	248	280
Ref. [46]	196–230	208–254	
Ref. [47]	200	249 (T_{80})	

catalyst studied previously [49], synthesized by chemical reaction between $Mn(NO_3)$ and $KMnO_4$, composed of α-MnO_2 and bixbyite α-Mn_2O_3 and with a specific area of 39 $m^2\ g^{-1}$. Indeed, the reference catalyst (Zn-free and sulfate-free) presents a lower T_{100} for ethanol oxidation than the MnO_x catalyst studied here. This oxide also presents the couple Mn^{3+}-Mn^{4+}, and the better conversion could be associated with the absence of Zn and sulfate species. Nevertheless, acetaldehyde production in this catalyst is higher than that of the MnO_x obtained using spent alkaline and Zn/C batteries. It is worth nothing that the conversion of VOCs in the catalysts prepared in this work is not so different from that of catalysts prepared using commercial salts. In addition, the production of incomplete oxidation products on MnO_x catalyst is low. These features render manganese catalysts prepared using spent alkaline and Zn/C batteries as raw material suitable for reducing oxygenated VOC emissions.

The reference manganese oxide was also studied in the oxidation of toluene, and results are presented in Fig. 7. In this case, the reference catalyst presents again a lower T_{100} for toluene

Please cite this article in press as: M.V. Gallegos et al., Removal of VOCs by catalytic process. A study of MnZnO composites synthesized from waste alkaline and Zn/C batteries, Chem. Eng. J. (2016), http://dx.doi.org/10.1016/j.cej.2016.11.001

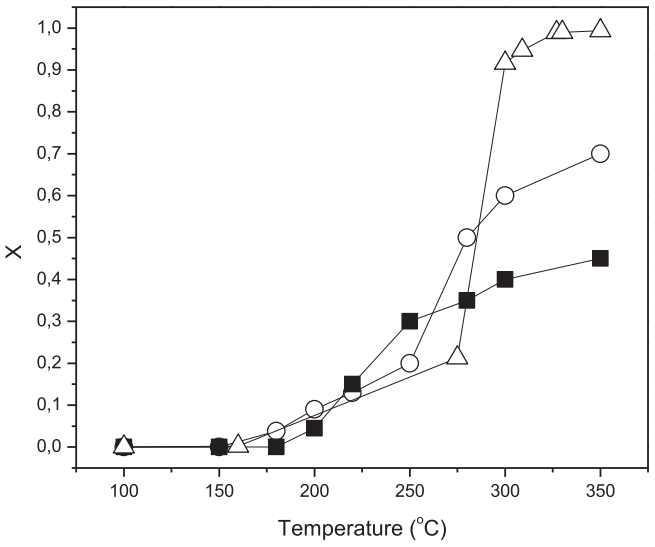

Fig. 7. Light-off curves of toluene oxidation over prepared catalysts: ■ ZnMnO; ○ MnO_x, △ Reference MnO_x catalyst. ($X = 1 - F_{Tol}/F_{Tol,in}$).

combustion than the MnO_x synthesized in this work, probably due to the absence of Zn and sulfate species.

3.3. Infrared studies

The spectra of all the pure catalyst disks present a clear strong absorption band in the region 1100–1200 cm^{-1}, which is assigned to the S=O stretching mode of sulfate species (exemplified in Fig. 8. a for the sample MnO_x). This band is more or less complex, showing several components. The position of the main maximum is similar to that observed in the case of the KBr disk spectrum. This position and the similarity of the KBr spectrum (recorded in air) to that of the pure powder pressed disk (recorded in vacuum after previous outgassing at 500 °C) suggest that it is due at least in part to highly coordinated sulfates present in the bulk of the solid. In fact, surface sulfates usually absorb at 1400–1200 cm^{-1} [52], i.e., at higher frequency than bulk sulfates. The IR spectra of the catalyst disk show, at the lower frequency side, the cutoff typically due to the bulk metal-oxygen vibrations near 700 cm^{-1} [53].

3.3.1. Adsorption of ethanol

The oxidation of ethanol performed in static conditions on the IR cell both, in the presence and in the absence of air, has been followed studying the IR spectra of surface species and gas-phase species.

The results of this experiment performed on the MnO_x sample in the absence of air are reported in Fig. 8. After ethanol adsorption at r.t. a weak absorption band is found near 1030 cm^{-1}, overlapping the strong sulfate band, which can be assigned to CO/CC stretching of surface alkoxy groups. This absorption band disappears progressively above 250 °C, when weak bands at 1550 and 1430 cm^{-1} form, due to surface acetates (COO asymmetric and symmetric stretchings modes, respectively). In order to evidence the newly formed adsorbed species, in Fig. 9 the subtraction spectra are reported. These spectra are obtained by subtracting the spectrum of MnO_x surface outgassed at high temperature from the spectrum of the surface in the presence of ethanol at the reported temperature. The spectral analysis confirms that ethoxy groups form upon ethanol absorption (positive band in the spectrum 9.a) and disappear when surface acetate species and acetaldehyde form (negative band of ethoxy groups and positive band of acetate species in the spectrum 9.b). The sequence of the spectra suggests that ethoxy groups are precursors of acetaldehyde formation while acetate species are not, being still observed at 380 °C. During these phenomena, the spectra of the catalyst change significantly near the cut off region, in comparison with the spectrum of the surface after heating in vacuum at high temperature (spectrum a in Fig. 8). Here, absorption in the region 800–600 cm^{-1} decreases very much and the cut off shifts to lower frequencies. A sharp band appears at 615 cm^{-1}, which is typical of manganite spinels (Fig. 8.h). The overall observations indicate that the catalyst bulk acts as an oxidant, allowing the oxidation of ethoxy species to acetaldehyde (which desorbs) and acetate species, reducing itself from MnO_2 to Mn_3O_4. In the absence of oxygen acetate species are stable on the surface at 380 °C. Correspondingly, in the gas phase spectra (Figs. 10 and 11), besides bands characterizing ethanol vapor at 3600 cm^{-1} (OH stretching mode), 3000–2800 cm^{-1} (CH stretching modes) and 1100–1000 cm^{-1} (CC/CO stretching modes), new bands are detected, corresponding to the formation of reaction products. In these conditions, the oxidation of ethanol starts at 250 °C with the formation of acetaldehyde (bands at 1700 cm^{-1}, C=O stretching mode, and at 2700 cm^{-1}, CH stretching with Fermi resonance band). On the

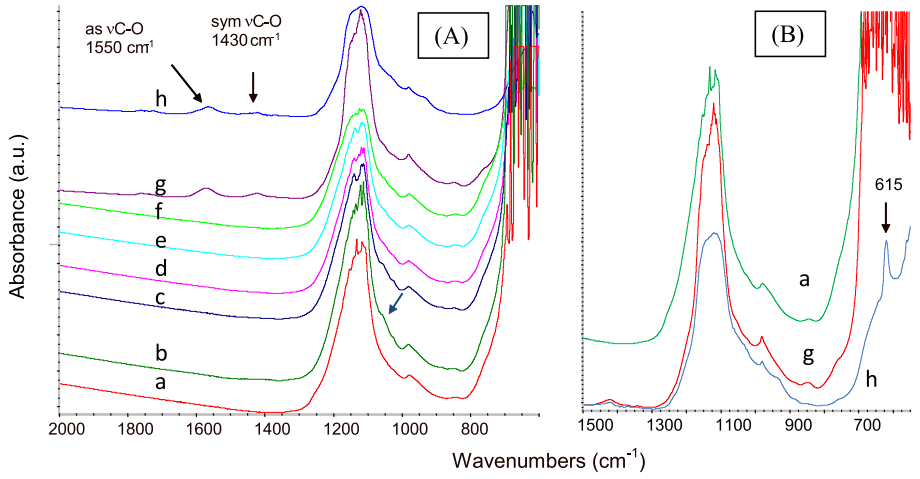

Fig. 8. FT IR spectra of surface species arising from ethanol adsorption and conversion over MnO_x catalyst (no air) (A): at (a) surface outgassed at 500 °C, (b) after ethanol adsorption at 25 °C, (c) at 100 °C, (d) at 150 °C, (e) at 200 °C, (f) 250 °C, (g) 340 °C and (h) at 380 °C. (B) Detail of the low frequency region: Mn-O stretching modes.

Please cite this article in press as: M.V. Gallegos et al., Removal of VOCs by catalytic process. A study of MnZnO composites synthesized from waste alkaline and Zn/C batteries, Chem. Eng. J. (2016), http://dx.doi.org/10.1016/j.cej.2016.11.001

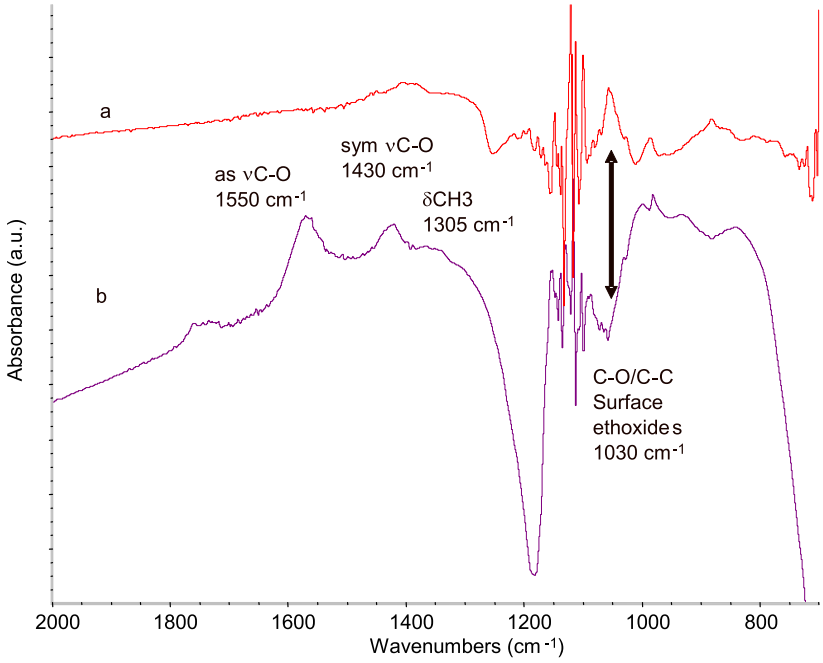

Fig. 9. FT IR subtraction spectra of surface species arising from ethanol adsorption over MnO_x catalyst at 25 °C (a) and at 380 °C (b). The activated surface has been subtracted.

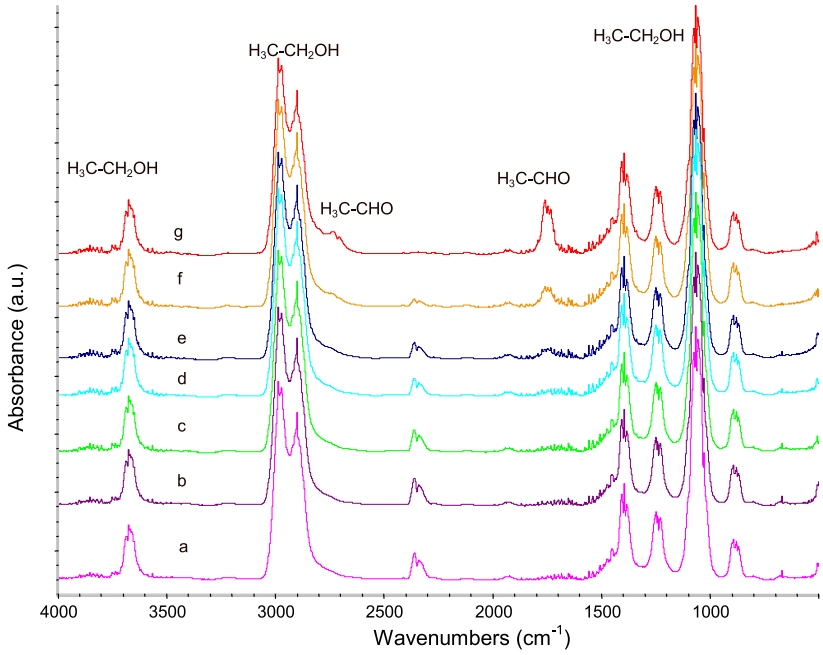

Fig. 10. FT IR spectra of gas phase species arising from ethanol conversion over MnO_x catalyst (no air) at (a) 25 °C, (b) 100 °C, (c) 150 °C, (d) 200 °C, (e) 250 °C, (f) 300 °C and (g) 380 °C.

other side, bands due to residual unreacted ethanol are still detected.

The subtraction spectra also show that the spectrum of the sulfate species undergoes some slightly changes, with the disappearance of a band at 1250 cm^{-1} upon adsorption of ethanol. This indicates that part of the sulfate band is due to surface sulfate species, characterized by the S=O stretching at the higher frequency side. This band is surface sensitive, being shifted to lower frequencies (similar to those of bulk sulfates) upon ethanol adsorption. Surface sulfate species may consequently be involved in the adsorption and conversion of ethanol.

In the experiment performed in the IR cell with some oxygen in the cell, acetaldehyde forms in the same temperature region as in the experiment performed without oxygen gas (Fig. 10), showing that reticular oxygen is likely involved in ethanol oxidative dehydrogenation. At 400 °C, however, CO_2 forms in significant amounts, while CO and CH_4 are also observed. Correspondingly ethanol bands are not detected anymore. Likely, in our static conditions, some by-products such as CO and methane are formed due to the high VOC/O_2 ratio, and possibly arising from a limited fraction of acetaldehyde molecules which undergo a parallel conversion path.

Please cite this article in press as: M.V. Gallegos et al., Removal of VOCs by catalytic process. A study of MnZnO composites synthesized from waste alkaline and Zn/C batteries, Chem. Eng. J. (2016), http://dx.doi.org/10.1016/j.cej.2016.11.001

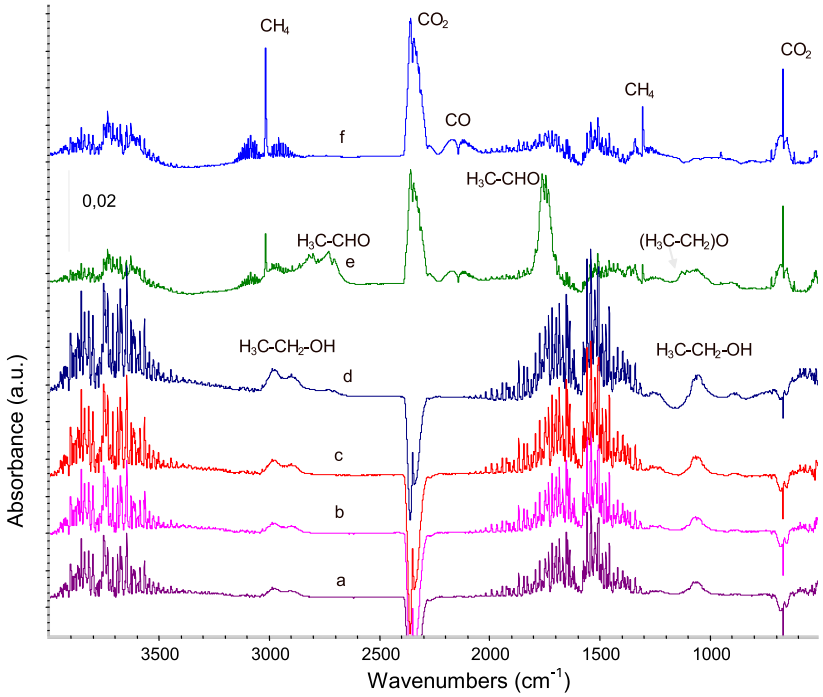

Fig. 11. FT IR spectra of gas phase species arising from ethanol conversion over MnO_x (in the presence of air) at (a) 25 °C, (b) 100 °C, (c) 200 °C, (d) 300 °C, (e) 400 °C and (f) 500 °C.

The spectra of the adsorbed species show again the formation of ethoxy groups at low temperature and of acetate species at higher temperature (Fig. 12). Also, in this case the absorption associated with the Mn-oxygen modes is slightly reduced at high temperature. This indicates that gas phase oxygen is needed to convert ethanol to CO_2, with the intermediacy of acetaldehyde in the 250–400 °C temperature range. If oxygen is not sufficient, acetaldehyde can decompose to $CO + CH_4$ instead of burning to CO_2, as reported above.

The data from these experiments compare well with the data on the catalytic conversion of ethanol. These data show that ethanol can be efficiently burnt catalytically over this catalyst, but the

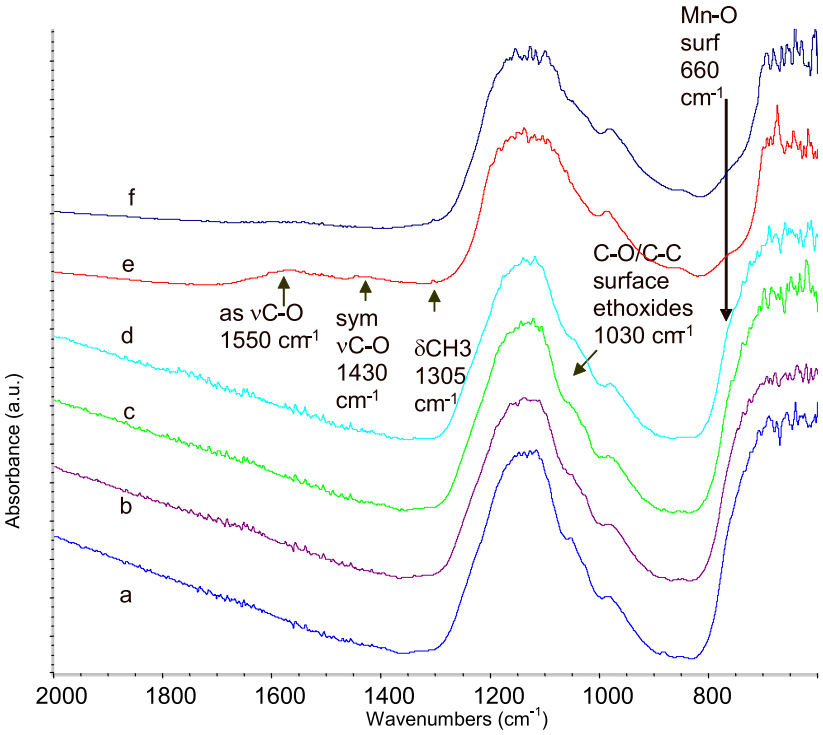

Fig. 12. FT IR spectra of surface species arising from ethanol adsorption and conversion over MnO_x catalyst (in the presence of air) at: (a) 25 °C, (b) 100 °C, (c) 200 °C, (d) 300 °C, (e) 400 °C and (f) 500 °C.

Please cite this article in press as: M.V. Gallegos et al., Removal of VOCs by catalytic process. A study of MnZnO composites synthesized from waste alkaline and Zn/C batteries, Chem. Eng. J. (2016), http://dx.doi.org/10.1016/j.cej.2016.11.001

reaction must be performed at 350 °C minimum temperature to avoid the formation of acetaldehyde, an unwanted VOC by-product.

The experiments of ethanol oxidation carried out in static conditions in the IR cell performed on the ZnMnO sample in general show similar results as in the case of MnO_x. As comparison, Fig. 13 shows the gas phase spectra of ethanol oxidation in the absence of air, over the ZnMnO sample. As in the MnO_x sample, the bands at 3600 cm^{-1}, 3000–2800 cm^{-1} and 1100–1000 cm^{-1} are characteristic of ethanol vapor, corresponding to OH, CH and CC/CO stretching modes, respectively. The formation of acetaldehyde (1700 cm^{-1} and 2700 cm^{-1}) starts at 350 °C in these conditions, i.e. 100 °C above the temperature at which it starts in the MnO_x sample.

The results of the ethanol oxidation over the Mn-based catalysts in the presence of air are in agreement with a previous work [49], where the adsorption-oxidation of ethanol in air over a manganese oxides, synthesized using commercial $Mn(NO_3)_2$ and $KMnO_4$ aqueous solutions, was studied. It was demonstrated that the oxidation of ethanol in air over a manganese oxide occurs from ethanol adsorption and the oxidation to acetaldehyde or CO_2 as a function of the temperature. In the catalysts prepared in this work, the analysis of catalytic tests and IR spectroscopy results suggest that combustion reaction mechanism follows a completely consistent path:

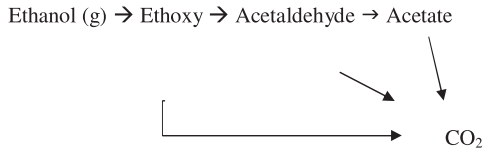

Adsorbed acetate species can also behave as reaction intermediate and be oxidized directly to CO_2 at high temperature.

When the temperature rises to 350–400 °C, CO and CH_4 are also detected in the IR experiment, together with CO_2 and likely due to the decomposition of acetaldehyde at high temperature in our experimental conditions [54,55].

The study without oxygen evidences that over the MnO_x catalysts ethanol adsorption gives rise to surface ethoxy and acetate species. The former are desorbed to the phase gas as acetaldehyde and then the aldehyde is oxidized to CO_2. On the other hand, in absence of oxygen acetate species are quite stable at the surface at high temperature and are not further oxidized, thus acting as spectator species. These results are in agreement with the catalytic activity without O_2 (Figs. 5 and 6).

3.3.2. Adsorption of toluene

Analogous studies have been performed using toluene as the reactant. In Fig.14 the IR spectra obtained with the catalyst MnO_x in the presence of air are reported. The corresponding spectra of gas-phase species are shown in Fig. 15. In this figure, the toluene molecule is characterized by two groups of CH stretching bands, above and below 3000 cm^{-1}, corresponding to CH stretching modes of aromatic and aliphatic CH groups, respectively [56]. Another set of sharp and weaker bands are detected between 1450 and 1600 cm^{-1}, due to the ring vibrational modes. The strong band around 750 cm^{-1} is typical of the mono substituted aromatic ring [56]. These bands slightly decrease in intensity above 250 °C. Toluene starts to be significantly converted into CO_2 at 300 °C, when the band of CO_2 (2350 cm^{-1}) starts to grow in the gas phase spectra. At 400 °C, CO is also observed (band at 2150 cm^{-1}) but its formation should be related to the reaction conditions in the IR cell (i.e. high content of VOC) No other species are observed in the gas phase. Looking at the surface species, bands at 1600, 1550 and 1430 cm^{-1} are observed already at 150 °C, and decrease in intensity progressively starting from 300 °C (Fig. 14). This is the typical behavior of the surface intermediate that forms on the surface before the reaction starts and disappears when reactions start to be fast. These bands could be assigned to carboxylate (likely benzoate) species [40], therefore suggesting that toluene conversion occurs first through oxidation at the methyl group, which results

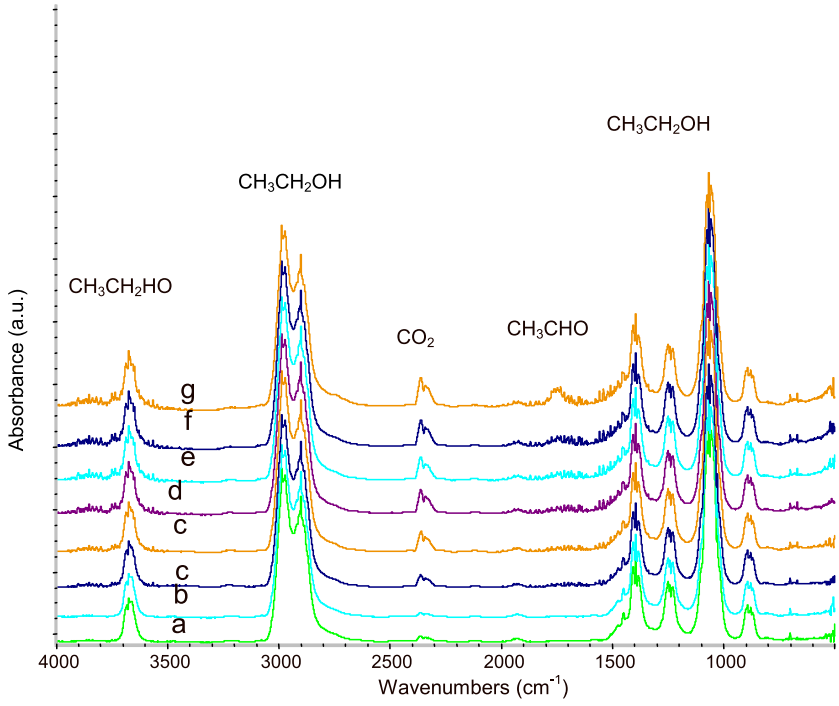

Fig. 13. FT IR spectra of gas phase species arising from ethanol conversion over ZnMnO catalyst (no air) at (a) 25 °C, (b) 100 °C, (c) 150 °C, (d) 200 °C, (e) 250 °C, (f) 300 °C and (g) 380 °C.

Please cite this article in press as: M.V. Gallegos et al., Removal of VOCs by catalytic process. A study of MnZnO composites synthesized from waste alkaline and Zn/C batteries, Chem. Eng. J. (2016), http://dx.doi.org/10.1016/j.cej.2016.11.001

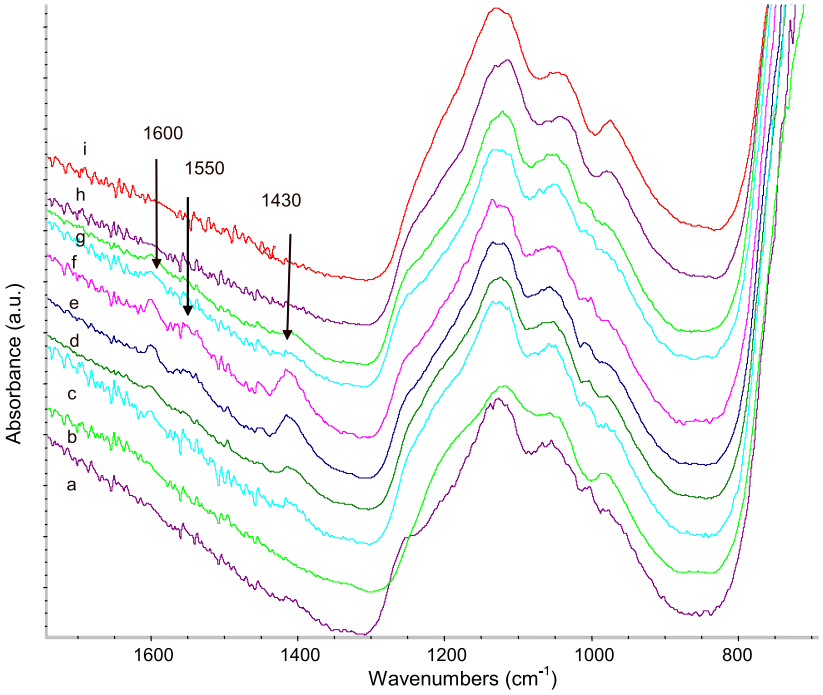

Fig. 14. FT IR spectra of surface species arising from toluene adsorption and conversion over MnO_x catalyst (in the presence of air): (a) activated surface, (b) 25 °C, (c) 100 °C, (d) 150 °C, (e) 200 °C, (f) 250 °C, (g) 300 °C, (h) 350 °C, (i) 400 °C and (j) 500 °C.

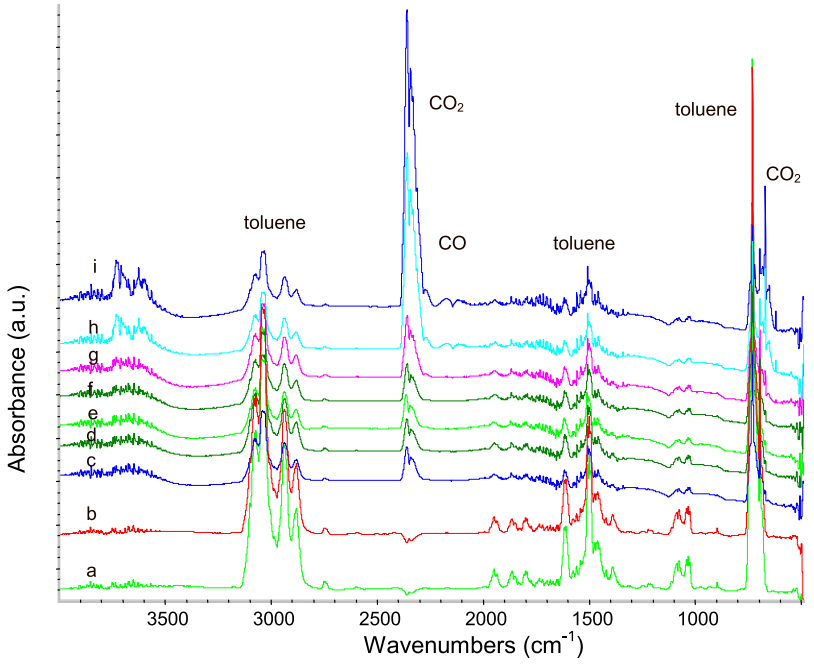

Fig. 15. FT IR spectra of gas phase species arising from toluene conversion over MnO_x (in the presence of air) at: (a) 25 °C, (b) 100 °C, (c) 150 °C, (d) 200 °C, (e) 250 °C, (f) 300 °C, (g) 350 °C, (h) 400 °C and (i) 500 °C.

in strong adsorption on the catalyst, followed by burning of the ring at higher temperatures (above 200 °C) to CO_2 and CO. No intermediate species having lower oxidation degree such as alkoxides or aldehydes could be detected. These species are likely formed but at a temperature at which further oxidation immediately occurs, as already reported in some early work on VOC combustion [57].

The oxidation of toluene in the IR cell performed on ZnMnO is represented in Fig.16. In the gas phase spectra, apart from some residual toluene, CO_2 and traces of CO at the highest temperatures, no other species are detected. Apparently, over this catalyst CO_2 and CO are formed in lower amount in comparison with the MnO_x catalyst (see Fig. 15), in agreement with activity tests evidencing the remarkably higher activity of MnO_x in toluene oxidation.

With respect to toluene oxidation our results are in agreement with the conclusion of Sun et al. [58], who have proposed that toluene is adsorbed like benzoate species. Different authors

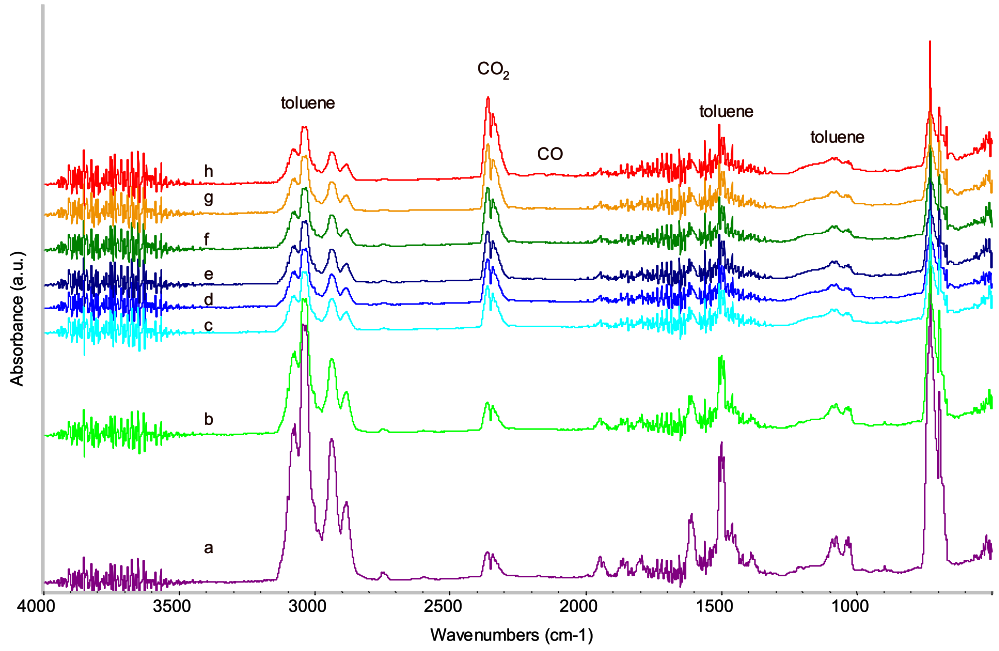

Fig. 16. FT IR spectra of gas phase species arising from toluene conversion over ZnMnO (in the presence of air) at: (a) 25 °C, (b) 100 °C, (c) 150 °C, (d) 200 °C, (e) 250 °C, (f) 350 °C, (g) 400 °C and (h) 500 °C.

[46,59,60] have shown that the toluene is stable on the surface of the manganese oxides and the total oxidation is reached between 240 and 300 °C. The MnO_x catalyst synthesized in this work, which is a recycled solid, reaches complete toluene oxidation at 250 °C without formation of partial oxidation products. This result is very interesting because waste batteries, which are a serious environmental problem, can be used as raw materials to prepared different manganese oxides, which can be used as efficient catalysts for the total oxidation of volatile organic compounds emissions.

4. Conclusions

MnO_x and ZnMnO solid catalysts have been obtained from spent alkaline and zinc–carbon batteries by an innovative biohydrometallurgical process.

XRD, XPS and TPR analysis indicates that MnO_x is constituted of α-MnO_2 and Mn_2O_3 phases, with the presence of Zn^{2+} and the Mn^{3+}-Mn^{4+} couple; whereas ZnMnO is composed of ZnO, $ZnMnO_3$ and Mn_2O_3. The higher OII/OI ratio was found on MnO_x oxide.

In spite of the presence of Zn^{2+} and surface sulfate formation from the recovery procedure, the MnO_x catalyst shows interesting activity in ethanol combustion and also in the most difficult toluene combustion in the temperature range 150–300 °C. The contemporary presence of Mn ions having different oxidation states and of mobile oxygen species is required for an efficient catalytic activity. Although ZnMnO also has the Mn^{3+}-Mn^{4+} couple, the better performance of MnO_x is due to the higher Mn/Zn ratio and the absence of ZnO.

The FTIR spectra show that ethanol adsorbs mainly in the form of ethoxides at the surface of the catalysts. Acetates are actually intermediates rather than spectators in the catalytic oxidation of ethanol over the oxides prepared from waste batteries in the presence of air. In the absence of air, the role of lattice oxygen in the oxidation process has been evidenced. In toluene oxidation, carboxylate species (benzoates) are likely reaction intermediates for total oxidation.

New manganese and zinc based catalysts for VOCs removal could be synthesized using spent alkaline and zinc–carbon batteries as starting materials.

Acknowledgements

Funding by the Italy (MAE)-Argentina (MINCYT, Project IT-1304) exchange program is gratefully acknowledged. The authors acknowledge the CONICET and UNLP (Argentina). We are thankful to Lic. P. Fetsis, Sra. Graciela Valle and Lic. M. Theiller. This work was supported by CONICET (PIP 942), CICPBA and ANPCyT (PICT 2012-2366) – Argentina.

References

[1] S.A.C. Carabineiro, D.T. Thompson, Catalytic applications for gold nanotechnology, in: U. Heiz, U. Landman (Eds.), Nanocatalysis, Springer, Berlin Heidelberg, New York, 2007, pp. 377–489.
[2] S.A.C. Carabineiro, X. Chen, M. Konsolakis, A.C. Psarras, P.B. Tavares, J.J.M. Órfão, M.F.R. Pereira, J.L. Figueiredo, Catalytic oxidation of toluene on Ce–Co and La–Co mixed oxides synthesized by exotemplating and evaporation methods, Catal. Today 244 (2015) 161–171, http://dx.doi.org/10.1016/j.cattod.2014.06.018.
[3] S.C. Kim, Y.K. Park, J.W. Nah, Property of a highly active bimetallic catalyst based on a supported manganese oxide for the complete oxidation of toluene, Powder Technol. 266 (2014) 292–298, http://dx.doi.org/10.1016/j.powtec.2014.06.049.
[4] J.E. Colman-Lerner, M.A. Peluso, A. Porta, H.J. Thomas, J.E. Sambeth, Catalytic removal of a mixture of volatile organic compounds present in indoor air at various work sites over Pt, MnO_x and Pt/MnO_x supported monoliths, React. Kinet. Mech. Catal. 114 (2015) 395–407, http://dx.doi.org/10.1007/s11144-014-0827-7.
[5] R. Craciun, Structure and redox properties of MnO_x/Yttrium-stabilized zirconia (YSZ) catalyst and its used in CO and CH_4 oxidation, Appl. Catal. A Gen. 243 (2003) 67–79, http://dx.doi.org/10.1016/S0926-860X(02)00538-0.
[6] M. Piumetti, D. Fino, N. Russo, Mesoporous manganese oxides prepared by solution combustion synthesis as catalysts for the total oxidation of VOCs, Appl. Catal. B Environ. 163 (2015) 277–287, http://dx.doi.org/10.1016/j.apcatb.2014.08.012.
[7] M.A. Peluso, L.A. Gambaro, E. Pronsato, D. Gazzoli, H.J. Thomas, J.E. Sambeth, Synthesis and catalytic activity of manganese dioxide (type OMS-2) for the abatement of oxygenated VOCs, Catal. Today 133–135 (2008) 487–492, http://dx.doi.org/10.1016/j.cattod.2007.12.132.
[8] K.C. Barick, S. Singh, M. Aslam, D. Bahadur, Porosity and photocatalytic studies of transition metal doped ZnO nanoclusters, Microporous Mesoporous Mater. 134 (2010) 195–202, http://dx.doi.org/10.1016/j.micromeso.2010.05.026.

Please cite this article in press as: M.V. Gallegos et al., Removal of VOCs by catalytic process. A study of MnZnO composites synthesized from waste alkaline and Zn/C batteries, Chem. Eng. J. (2016), http://dx.doi.org/10.1016/j.cej.2016.11.001

[9] R. Kumar, A. Umar, G. Kumar, M.S. Akhtar, Y. Wang, S.H. Kim, Ce-doped ZnO nanoparticles for efficient photocatalytic degradation of direct red-23 dye, Ceram. Int. 41 (2015) 7773–7782, http://dx.doi.org/10.1016/j.ceramint.2015.02.110.

[10] W. Cai, P.R. de la Piscina, N. Homs, Oxidative steam reforming of bio-butanol for hydrogen production: effects of noble metals on bimetallic CoM/ZnO catalysts (M=Ru, Rh, Ir, Pd), Appl. Catal. B Environ. 145 (2014) 56–62, http://dx.doi.org/10.1016/j.apcatb.2013.03.016.

[11] J.A. Torres, J. Llorca, A. Casanovas, M. Domínguez, J. Salvadó, D. Montané, Steam reforming of ethanol at moderate temperature: multifactorial design analysis of Ni/La_2O_3-Al_2O_3, and Fe- and Mn-promoted Co/ZnO catalysts, J. Power Sources 169 (2007) 158–166, http://dx.doi.org/10.1016/j.jpowsour.2007.01.057.

[12] H. Lei, R. Nie, G. Wu, Z. Hou, Hydrogenation of CO_2 to CH_3OH over Cu/ZnO catalysts with different ZnO morphology, Fuel 154 (2015) 161–166, http://dx.doi.org/10.1016/j.fuel.2015.03.052.

[13] B. Donkova, D. Dimitrov, M. Kostadinov, E. Mitkova, D. Mehandjiev, Catalytic and photocatalytic activity of lightly doped catalysts M:ZnO (M = Cu, Mn), Mater. Chem. Phys. 123 (2010) 563–568, http://dx.doi.org/10.1016/j.matchemphys.2010.05.015.

[14] J. Chen, C. Tang, Preparation and application of granular ZnO/Al_2O_3 catalyst for the removal of hazardous trichloroethylene, J. Hazard. Mater. 142 (2007) 88–96, http://dx.doi.org/10.1016/j.jhazmat.2006.07.061.

[15] M. Ashokkumar, S. Muthukumaran, Enhanced room temperature ferromagnetism and photoluminescence behavior of Cu-doped ZnO co-doped with Mn, Phys. E Low-Dimension. Syst. Nanostruct. 69 (2015) 354–359, http://dx.doi.org/10.1016/j.physe.2015.02.010.

[16] R. Mimouni, O. Kamoun, A. Yumak, A. Mhamdi, K. Boubaker, P. Petkova, M. Amlouk, Effect of Mn content on structural, optical, opto-thermal and electrical properties of ZnO:Mn sprayed thin films compounds, J. Alloys Compd. 645 (2015) 100–111, http://dx.doi.org/10.1016/j.jallcom.2015.05.012.

[17] B. Zeytuncu, Dissolution of alkaline batteries in reductive acidic media, Physicochem. Probl. Miner. Process. 52 (2016) 437–450, http://dx.doi.org/10.5277/ppmp160136.

[18] Y. Ma, Y. Cui, X. Zuo, S. Huang, K. Hu, X. Xiao, J. Nan, Reclaiming the spent alkaline zinc manganese dioxide batteries collected from the manufacturers to prepare valuable electrolytic zinc and LiNi0.5Mn1.5O_4 materials, Waste Manag. 34 (2014) 1793–1799, http://dx.doi.org/10.1016/j.wasman.2014.05.009.

[19] Directive 2006/66/EC of the European Parliament and of the Council of 6 September 2006 on batteries and accumulators and waste batteries and accumulators and repealing Directive 91/157/EEC, Off. J. Eur. Union. L 266 (2006) 1–14, doi:12.12.2013.

[20] W. Wu, P. Bromberg, J.M. Samet, Zinc ions as effectors of environmental oxidative lung injury, Free Radic. Biol. Med. 65 (2013) 57–69, http://dx.doi.org/10.1016/j.freeradbiomed.2013.05.048.

[21] B. Chen, J. Luo, M. Hendryx, Zinc compound air releases from toxics release inventory facilities and cardiovascular disease mortality rates, Environ. Res. 142 (2015) 96–103, http://dx.doi.org/10.1016/j.envres.2015.06.022.

[22] M.P. Tavlieva, S.D. Genieva, V.G. Georgieva, L.T. Vlaev, Thermodynamics and kinetics of the removal of manganese(II) ions from aqueous solutions by white rice husk ash, J. Mol. Liq. 211 (2015) 938–947, http://dx.doi.org/10.1016/j.molliq.2015.08.015.

[23] Greenpeace Argentina, y BateriasGestion de Residuos de Pilas y Baterias, Buenos Aires, 2010. http://www.greenpeace.org/argentina/Global/argentina/report/2010/7/informe-gestion-pilas-baterias.pdf.

[24] Dirección de Residuos Peligrosos Dirección Nacional de Control Ambiental Subsecretaría de Control y Fiscalización Ambiental y Prevención de la Contaminación Pilas en Argentina, Buenos Aires, 2010. www.ambiente.org.ar.

[25] R.K. Biswas, A.K. Karmakar, S.L. Kumar, M.N. Hossain, Recovery of manganese and zinc from waste Zn–C cell powder: characterization and leaching, Waste Manag. 46 (2015) 4–10, http://dx.doi.org/10.1016/j.wasman.2015.09.008.

[26] D.C.R. Espinosa, A.M. Bernardes, J.A.S. Tenório, An overview on the current processes for the recycling of batteries, J. Power Sources 135 (2004) 311–319, http://dx.doi.org/10.1016/j.jpowsour.2004.03.083.

[27] C.L. Brierley, Biohydrometallurgical prospects, Hydrometallurgy 104 (2010) 324–328, http://dx.doi.org/10.1016/j.hydromet.2010.03.021.

[28] M.A. Gabal, R.S. Al-luhaibi, Y.M. Al Angari, Recycling spent zinc–carbon batteries through synthesizing nano-crystalline Mn–Zn ferrites, Powder Technol. 258 (2014) 32–37, http://dx.doi.org/10.1016/j.powtec.2014.03.003.

[29] Y. Song, Q. Huang, Z. Niu, J. Ma, B. Xin, S. Chen, J. Dai, R. Wang, Preparation of Zn–Mn ferrite from spent Zn–Mn batteries using a novel multi-step process of bioleaching and co-precipitation and boiling reflux, Hydrometallurgy 153 (2015) 66–73, http://dx.doi.org/10.1016/j.hydromet.2015.02.007.

[30] M.V. Gallegos, L.R. Falco, M.A. Peluso, J.E. Sambeth, H.J. Thomas, Recovery of manganese oxides from spent alkaline and zinc-carbon batteries. An application as catalysts for VOCs elimination, Waste Manag. 33 (2013) 1483–1490, http://dx.doi.org/10.1016/j.wasman.2013.03.006.

[31] L.R. Falco, A. Martinez, M. Di Nanno, H. Thomas, G. Curutchet, Study of a pilot plant for the recovery of metals from spent alkaline and zinc-carbon batteries with biological sulphuric acid and polythionate production, Lat. Am. Appl. Res. 44 (2014) 123–129.

[32] C. Julien, Lattice vibrations of manganese oxides Part I. Periodic structures, Spectrochim. Acta Part A Mol. Biomol. Spectrosc. 60 (2004) 689–700, http://dx.doi.org/10.1016/S1386-1425(03)00279-8.

[33] P. Zhang, X. Li, Q. Zhao, S. Liu, Synthesis and optical property of one-dimensional spinel $ZnMn_2O_4$ nanorods, Nanoscale Res. Lett. 6 (2011) 323, http://dx.doi.org/10.1186/1556-276X-6-323.

[34] X. Guo, H.-S. Xiao, F. Wang, Y.-H. Zhang, Micro-Raman and FTIR spectroscopic observation on the phase transitions of $MnSO_4$ droplets and ionic interactions between Mn^{2+} and SO_4^{2-}, J. Phys. Chem. A 114 (2010) 6480–6486, http://dx.doi.org/10.1021/jp9104147.

[35] C. Cong, L. Liao, C. Li, L. Fan, K. Zhang, Synthesis, structure and ferromagnetic properties of Mn-doped ZnO nanoparticles, Nanotechnology 16 (2005) 981–984, http://dx.doi.org/10.1088/0957-4484/16/6/060.

[36] U. Ilyas, R.S. Rawat, G. Roshan, T.L. Tan, P. Lee, S.V. Springham, S. Zhang, L. Fengji, R. Chen, H.D. Sun, Quenching of surface traps in Mn doped ZnO thin films for enhanced optical transparency, Appl. Surf. Sci. 258 (2011) 890–897, http://dx.doi.org/10.1016/j.apsusc.2011.09.021.

[37] W. Xiao, Q. Chen, Y. Wu, T. Wu, L. Dai, Ferromagnetism of $Zn_{0.95}Mn_{0.05}O$ controlled by concentration of zinc acetate in ionic liquid precursor, Mater. Chem. Phys. 123 (2010) 1–4, http://dx.doi.org/10.1016/j.matchemphys.2010.04.007.

[38] V.E.O. Santos, V.G. Celante, M.F.F. Lelis, M.B.J.G. Freitas, Chemical and electrochemical recycling of the nickel, cobalt, zinc and manganese from the positives electrodes of spent Ni–MH batteries from mobile phones, J. Power Sources 218 (2012) 435–444, http://dx.doi.org/10.1016/j.jpowsour.2012.07.024.

[39] Y. Liu, H. Dai, J. Deng, S. Xie, H. Yang, W. Tan, W. Han, Y. Jiang, G. Guo, Mesoporous Co_3O_4-supported gold nanocatalysts: highly active for the oxidation of carbon monoxide, benzene, toluene, and o-xylene, J. Catal. 309 (2014) 408–418, http://dx.doi.org/10.1016/j.jcat.2013.10.019.

[40] C.-J. Li, G.-R. Xu, Zn–Mn–O heterostructures: study on preparation, magnetic and photocatalytic properties, Mater. Sci. Eng., B 176 (2011) 552–558, http://dx.doi.org/10.1016/j.mseb.2011.01.011.

[41] D. Dobber, D. Döbber, D. Kießling, W. Schmitz, G. Wendt, MnOx/ZrO_2 catalysts for the total oxidation of methane and chloromethane, Appl. Catal. B Environ. 52 (2004) 135–143, http://dx.doi.org/10.1016/j.apcatb.2004.02.012.

[42] M. Liang, W. Kang, K. Xie, Comparison of reduction behavior of Fe_2O_3, ZnO and $ZnFe_2O_4$ by TPR technique, J. Nat. Gas Chem. 18 (2009) 110–113, http://dx.doi.org/10.1016/S1003-9953(08)60073-0.

[43] M.A. Valenzuela, P. Bosch, J. Jiménez-Becerrill, O. Quiroz, A.I. Páez, Preparation, characterization and photocatalytic activity of ZnO, Fe_2O_3 and $ZnFe_2O_4$, J. Photochem. Photobiol. A Chem. 148 (2002) 177–182, http://dx.doi.org/10.1016/S1010-6030(02)00040-0.

[44] Z. Wu, R. Jin, Y. Liu, H. Wang, Ceria modified MnO_x/TiO_2 as a superior catalyst for NO reduction with NH_3 at low-temperature, Catal. Commun. 9 (2008) 2217–2220, http://dx.doi.org/10.1016/j.catcom.2008.05.001.

[45] D.A. Aguilera, A. Perez, R. Molina, S. Moreno, Cu-Mn and Co-Mn catalysts synthesized from hydrotalcites and their use in the oxidation of VOCs, Appl. Catal. B Environ. 104 (2011) 144–150, http://dx.doi.org/10.1016/j.apcatb.2011.02.019.

[46] V.P. Santos, M.F.R. Pereira, J.J.M. Órfão, J.L. Figueiredo, The role of lattice oxygen on the activity of manganese oxides towards the oxidation of volatile organic compounds, Appl. Catal. B Environ. 99 (2010) 353–363, http://dx.doi.org/10.1016/j.apcatb.2010.07.007.

[47] F.G. Durán, B.P. Barbero, L.E. Cadús, C. Rojas, M.Á. Centeno, J.A. Odriozola, Manganese and iron oxides as combustion catalysts of volatile organic compounds, Appl. Catal. B Environ. 92 (2009) 194–201, http://dx.doi.org/10.1016/j.apcatb.2009.07.010.

[48] H. Lüth, G.W. Rubloff, W.D. Grobman, Chemisorption of organic molecules on ZnO(1−1 0 0) surfaces: C_5H_5N, $(CH_3)_2CO$, and $(CH_3)_2SO$, Surf. Sci. 74 (1978) 365–372, http://dx.doi.org/10.1016/0039-6028(78)90033-X.

[49] M.A. Peluso, E. Pronsato, J.E. Sambeth, H.J. Thomas, G. Busca, Catalytic combustion of ethanol on pure and alumina supported K-Mn oxides: an IR and flow reactor study, Appl. Catal. B Environ. 78 (2008) 73–79, http://dx.doi.org/10.1016/j.apcatb.2007.09.002.

[50] A.R. Gandhe, J.S. Rebello, J.L. Figueiredo, J.B. Fernandes, Manganese oxide OMS-2 as an effective catalyst for total oxidation of ethyl acetate, Appl. Catal. B Environ. 72 (2007) 129–135, http://dx.doi.org/10.1016/j.apcatb.2006.10.017.

[51] V.P. Santos, S.A.C. Carabineiro, P.B. Tavares, M.F.R. Pereira, J.J.M. Órfão, J.L. Figueiredo, Oxidation of CO, ethanol and toluene over TiO_2 supported noble metal catalysts, Appl. Catal. B Environ. 99 (2010) 198–205, http://dx.doi.org/10.1016/j.apcatb.2010.06.020.

[52] S. Specchia, E. Finocchio, G. Busca, G. Saracco, V. Specchia, Effect of S-compounds on Pd over $LaMnO_3$·$2ZrO_2$ and CeO_2·$2ZrO_2$ catalysts for CH_4 combustion, Catal. Today 143 (2009) 86–93, http://dx.doi.org/10.1016/j.cattod.2008.10.035.

[53] G. Busca, Infrared Spectroscopy in Oxidation Catalysis, in: D. Duprez, F. Cavani (Eds.), Handb. Adv. Methods Process. Oxid. Catal., World Scientific, Singapore, 2014, pp. 447–495.

[54] J.W.C. Liberatori, R.U. Ribeiro, D. Zanchet, F.B. Noronha, J.M.C. Bueno, Steam reforming of ethanol on supported nickel catalysts, Appl. Catal. A Gen. 327 (2007) 197–204, http://dx.doi.org/10.1016/j.apcata.2007.05.010.

[55] T.S. Moraes, R.C. Rabelo Neto, M.C. Ribeiro, L.V. Mattos, M. Kourtelesis, S. Ladas, et al., Ethanol conversion at low temperature over CeO_2—Supported Ni-based catalysts. Effect of Pt addition to Ni catalyst, Appl. Catal. B Environ. 181 (2016) 754–768, http://dx.doi.org/10.1016/j.apcatb.2015.08.044.

[56] D. Lin-Vien, N.B. Colthup, W.G. Fateley, J.G. Grasselli, The Handbook of Infrared and Raman Characteristic Frequencies of Organic Molecules, Elsevier, 1991, http://dx.doi.org/10.1016/B978-0-08-057116-4.50023-7.

Please cite this article in press as: M.V. Gallegos et al., Removal of VOCs by catalytic process. A study of MnZnO composites synthesized from waste alkaline and Zn/C batteries, Chem. Eng. J. (2016), http://dx.doi.org/10.1016/j.cej.2016.11.001

[57] E. Finocchio, G. Busca, V. Lorenzelli, R.J. Willey, The activation of hydrocarbon CH bonds over transition metal oxide catalysts: a FTIR study of hydrocarbon catalytic combustion over $MgCr_2O_4$, J. Catal. 151 (1995) 204–215, http://dx.doi.org/10.1006/jcat.1995.1022.

[58] H. Sun, Z. Liu, S. Chen, X. Quan, The role of lattice oxygen on the activity and selectivity of the OMS-2 catalyst for the total oxidation of toluene, Chem. Eng. J. 270 (2015) 58–65, http://dx.doi.org/10.1016/j.cej.2015.02.017.

[59] H. Sun, S. Chen, P. Wang, X. Quan, Catalytic oxidation of toluene over manganese oxide octahedral molecular sieves (OMS-2) synthesized by different methods, Chem. Eng. J. 178 (2011) 191–196, http://dx.doi.org/10.1016/j.cej.2011.10.047.

[60] S.S.T. Bastos, S.A.C. Carabineiro, J.J.M. Orfao, M.F.R. Pereira, J.J. Delgado, J.L. Figueiredo, Total oxidation of ethyl acetate, ethanol and toluene catalyzed by exotemplated manganese and cerium oxides loaded with gold, Catal. Today 180 (2012) 148–154, http://dx.doi.org/10.1016/j.cattod.2011.01.049.

Please cite this article in press as: M.V. Gallegos et al., Removal of VOCs by catalytic process. A study of MnZnO composites synthesized from waste alkaline and Zn/C batteries, Chem. Eng. J. (2016), http://dx.doi.org/10.1016/j.cej.2016.11.001